Chasing the nonlinear evolution of matter power spectrum with a numerical resummation method: Solution of closure equations

Takashi Hiramatsu[1] and Atsushi Taruya[2,3]

[1]*Institute for Cosmic Ray Research, The University of Tokyo, Kashiwa, Chiba 277-8582, Japan*
[2]*Research Center for the Early Universe, School of Science, The University of Tokyo, Bunkyo-ku, Tokyo 113-0033, Japan*
[3]*Institute for the Physics and Mathematics of the Universe, The University of Tokyo, Kashiwa, Chiba 277-8568, Japan*

(Received 5 March 2009; published 27 May 2009)

We present a new numerical scheme to treat the nonlinear evolution of cosmological power spectra. Governing equations for matter power spectra have been previously derived by a nonperturbative technique with closure approximation. Solutions of the resultant closure equations just correspond to the resummation of an infinite class of perturbation corrections, and they consistently reproduce the one-loop results of standard perturbation theory. We develop a numerical algorithm to solve closure evolutions in both perturbative and nonperturbative regimes. The present numerical scheme is particularly suited for examining nonlinear matter power spectrum in general cosmological models, including modified theory of gravity. As a demonstration, we study weakly nonlinear evolution of power spectrum in a class of modified gravity models, as well as various dark energy models.

DOI: 10.1103/PhysRevD.79.103526 PACS numbers: 98.80.−k

I. INTRODUCTION

In the last decade, the late-time cosmic acceleration has been one of the most important discoveries in physics and cosmology (e.g., Refs. [1,2]). Although the origin of late-time acceleration is thought to be a mysterious energy component called dark energy, a possibility of long-distance modification of general relativity is still viable (e.g., Refs. [3,4]), and our understanding of the nature of late-time acceleration is still lacking. Currently, the dark energy equation-of-state parameter $w_{\rm de}$, which is phenomenologically introduced to characterize the cosmic acceleration and is defined as the ratio of the pressure to the energy density of dark energy, is consistent with a cosmological constant ($w_{\rm de} = -1$) at a level of 10% precision, and with no evidence for time dependence (e.g., Refs. [5,6]). Toward a deeper understanding of the nature of late-time acceleration, a precise measurement of both the cosmic expansion history and the growth of cosmic structure is a key to distinguish between different models of dark energy, as well as to discriminate the dark energy from the modification of gravity.

Among several observational techniques, baryon acoustic oscillations imprinted on matter power spectrum and cosmic shear, measured from galaxy samples, are the most promising techniques sensitive to the expansion history and growth of structure. A crucial remark is that they strongly rely on the accurate predictions of nonlinear matter power spectrum. Hence, in addition to the precise measurement, a high-precision theoretical template for the nonlinear power spectrum must be developed in order to achieve order-of-magnitude improvement of the current constraints.

Recently, several analytical approaches to predict the nonlinear power spectrum have been developed, complementary to the N-body simulations [7–13]. In contrast to the standard analytical calculation with perturbation theory (for a review, see Ref. [14]), these have been formulated in a nonperturbative way with techniques resumming a class of infinite series of higher-order corrections in perturbative calculation. Thanks to its nonperturbative formulation, the applicable range of the prediction has been greatly improved, and the nonlinear evolution of baryon acoustic oscillations was found to be accurately described with a percent-level precision.

Note, however, that these analytical calculations involve several approximations or simplifications in order to make the analysis tractable. This severely limits the applicable range and/or the versatility of predictions. For example, in Refs. [12,13], a perturbative treatment called Born approximation has been partly adopted in order to evaluate the nonperturbative expressions for power spectrum. Furthermore, most of the analysis presented so far rely on the Einstein-de Sitter approximation, in which all the calculations done in the Einstein-de Sitter universe are extended to apply to the other cosmological model by simply replacing the linear growth factor in Einstein-de Sitter universe with that in the other cosmology (see Sec. V B 1 in detail). This is very crucial in studying the nonlinear matter power spectrum in general cosmological models, especially in modified gravity models.

In the present paper, in order to bring out the advantage of nonperturbative formulation as much as possible, we present a numerical resummation scheme to calculate the nonlinear matter power spectrum. Our treatment relies on the formalism developed by Ref. [13], in which the nonlinear statistical method used in the subject of turbulence (e.g., Ref. [15]) was applied to the derivation of governing equations for power spectrum. The resultant equations called closure equations are the nonlinear integro-

differential equations coupled with nonlinear propagator. The solution of closure equations effectively contains the information of the higher-order corrections, similar to the renormalized perturbation theory by Crocce & Scoccimarro [7,8,12]. It has been shown that the analytical predictions based on the leading-order Born approximation agree with N-body simulations very well in a mildly nonlinear regime, and a percent-level precision was achieved at some ranges [16]. The agreement of the prediction is further improved if taking account of the next-to-leading order correction [17]. Hence, with the numerical implementation of the closure equations, all orders of Born approximation are included, and the prediction will be much better than the analytical treatment. Further, the numerical treatment is particularly suited for studying the nonlinear power spectrum in various cosmologies where the analytical calculations with Einstein-de Sitter approximation is no longer possible.

The paper is organized as follows. In Secs. II and III, we briefly review the basic treatment of our approach and formalism. We then discuss how to solve closure equations in Sec. IV. As shown in Ref. [13], the closure equations automatically reproduce the leading-order results of standard perturbation theory if replacing the quantities in nonlinear terms with linear-order ones. This treatment has been used for computing quasi nonlinear spectrum in modified gravity models in Ref. [18]. In Sec. V, we present numerical solutions of closure equations in both full nonlinear and perturbative treatment and demonstrate how the present scheme can treat analytically intractable cases. Finally, Sec. VI is devoted to the discussion and conclusion.

II. PRELIMINARIES

Throughout the paper, we consider the evolution of mass distribution in the flat universe, neglecting the tiny contributions from the massive neutrinos. We treat the cold dark matter (CDM) plus baryon system as a pressureless perfect fluid. Then, assuming the irrotationality of fluid flow, the governing equations for matter distribution become the continuity equation and the Euler equation coupled to the Newton potential ϕ (e.g., Ref. [14]) :

$$\frac{\partial\delta(\tau,\boldsymbol{x})}{\partial\tau}+\theta(\tau,\boldsymbol{x})=-\frac{1}{aH}\nabla\cdot(\delta\boldsymbol{v}), \tag{1}$$

$$\frac{\partial\theta(\tau,\boldsymbol{x})}{\partial\tau}+\left(2+\frac{d\ln H}{d\tau}\right)\theta(\tau,\boldsymbol{x}) =-\frac{1}{a^2H^2}\triangle\phi(\tau,\boldsymbol{x})-\frac{1}{a^2H^2}\nabla\cdot(\boldsymbol{v}\cdot\nabla\boldsymbol{v}), \tag{2}$$

where δ is the mass density field, and θ is the velocity divergence defined as $\theta\equiv\nabla\cdot\boldsymbol{v}/(aH)$. Here, we introduce the time variable given by $\tau=\log(a/a_0)$, with a_0 being the scale factor at the present time. With this time variable, the flat Friedmann equation becomes

$$H^2=H_0^2\left\{\Omega_{\rm m}e^{-3\tau}+\Omega_{\rm de}\exp\left[-3\int_0^\tau d\tau'\{1+w_{\rm de}(\tau')\}\right]\right\}. \tag{3}$$

The quantity H_0 is the Hubble parameter at the present time, and $\Omega_{\rm m}$ and $\Omega_{\rm de}$ are the density parameters of the matter and dark energy, respectively.

To treat the nonlinear evolution of matter power spectrum, we will work with the Fourier transform of the fluid equations, (1) and (2). They are given by

$$\frac{\partial\delta(\boldsymbol{k},\tau)}{\partial\tau}+\theta(\boldsymbol{k},\tau)=-\int\frac{d^3\boldsymbol{k}_1d^3\boldsymbol{k}_2}{(2\pi)^3}\delta_{\rm D}(\boldsymbol{k}-\boldsymbol{k}_1-\boldsymbol{k}_2) \times\left\{1+\frac{\boldsymbol{k}_1\cdot\boldsymbol{k}_2}{|\boldsymbol{k}_1|^2}\right\}\theta(\boldsymbol{k}_1,\tau)\delta(\boldsymbol{k}_2,\tau), \tag{4}$$

$$\frac{\partial\theta(\boldsymbol{k},\tau)}{\partial\tau}+\left(2+\frac{d\ln H}{d\tau}\right)\theta(\boldsymbol{k},\tau)-\left(\frac{k}{aH}\right)^2\phi(\boldsymbol{k},\tau) =-\int\frac{d^3\boldsymbol{k}_1d^3\boldsymbol{k}_2}{(2\pi)^3}\delta_{\rm D}(\boldsymbol{k}-\boldsymbol{k}_1-\boldsymbol{k}_2) \times\frac{(\boldsymbol{k}_1\cdot\boldsymbol{k}_2)|\boldsymbol{k}_1+\boldsymbol{k}_2|^2}{2|\boldsymbol{k}_1|^2|\boldsymbol{k}_2|^2}\theta(\boldsymbol{k}_1,\tau)\theta(\boldsymbol{k}_2,\tau). \tag{5}$$

As for the Poisson equation, we have

$$-\frac{k^2}{a^2}\phi(\boldsymbol{k},\tau)=4\pi G_{\rm eff}(\boldsymbol{k},\tau)\rho_{\rm m}\delta(\boldsymbol{k},\tau). \tag{6}$$

Here, $G_{\rm eff}$ is the effective Newton constant, which generically depends on the scale and time in modified theory of gravity. In principle, the Newton potential can be a nonlinear function of the density field. In fact, successful modified gravity models that explain late-time acceleration such as the Dvali-Gabadadze-Porrati (DGP) model [3] and $f(R)$ gravity models (for a review, see Ref. [4]) have nonlinear interaction terms, which are essential to recover the general relativity on small scales [19]. In the present paper, we restrict our analysis to the cases with linear Poisson equation. The extension to the nonlinear case is straightforward and is discussed in a separate paper [18].

The evolution Eqs. (4)–(6) can be further reduced to a compact form if we introduce the following quantity:

$$\Phi_a(\boldsymbol{k},\tau)=(\delta(\boldsymbol{k},\tau),-\theta(\boldsymbol{k},\tau)); \qquad (a=1,2). \tag{7}$$

Then, we write down the evolution equations in a single form as

$$\hat{\Lambda}_{ab}\Phi_b(\tau,\boldsymbol{k})=\frac{d^3\boldsymbol{k}_1d^3\boldsymbol{k}_2}{(2\pi)^6}\delta_D(\boldsymbol{k}_1+\boldsymbol{k}_2-\boldsymbol{k})\gamma_{acd}(\boldsymbol{k}_1,\boldsymbol{k}_2) \times\Phi_c(\boldsymbol{k}_1)\Phi_d(\boldsymbol{k}_2), \tag{8}$$

where γ_{acd} is the vertex function defined as

$$\gamma_{112}(\boldsymbol{k}_2,\boldsymbol{k}_1)=\gamma_{121}(\boldsymbol{k}_1,\boldsymbol{k}_2)=\frac{1}{2}\left(1+\frac{\boldsymbol{k}_1\cdot\boldsymbol{k}_2}{|\boldsymbol{k}_1|^2}\right),$$
$$\gamma_{222}(\boldsymbol{k}_1,\boldsymbol{k}_2)=\frac{1}{2}\left(\frac{|\boldsymbol{k}_1+\boldsymbol{k}_2|^2\boldsymbol{k}_1\cdot\boldsymbol{k}_2}{|\boldsymbol{k}_1|^2|\boldsymbol{k}_2|^2}\right). \quad (9)$$

The operator $\hat{\Lambda}_{ab}$ is defined by

$$\hat{\Lambda}_{ab}=\delta_{ab}\frac{\partial}{\partial\tau}+\Omega_{ab}(k,\tau), \quad (10)$$

with the matrix Ω_{ab} being

$$\Omega_{ab}(k,\tau)=\begin{pmatrix}0 & -1\\ -4\pi G_{\rm eff}\frac{\rho_{\rm m}}{H^2} & 2+\frac{d\ln H}{d\tau}\end{pmatrix}. \quad (11)$$

III. CLOSURE EQUATIONS

In the present paper, we are especially concerned with the nonlinear evolution of power spectrum defined by

$$\langle\Phi_a(\boldsymbol{k},\tau)\Phi_b(\boldsymbol{k}',\tau)\rangle=(2\pi)^3\delta_D(\boldsymbol{k}+\boldsymbol{k}')P_{ab}(|\boldsymbol{k}|;\tau), \quad (12)$$

where the bracket $\langle\cdot\rangle$ stands for ensemble average. In the above definition, we have the three different power spectra, P_{11}, $P_{12}=P_{21}$, and P_{22}, which, respectively, correspond to $P_{\delta\delta}$, $-P_{\delta\theta}$ and $P_{\theta\theta}$.

For the analytical calculation of the power spectrum, the standard treatment of perturbation theory is to expand the quantity Φ_a as $\Phi_a=\Phi_a^{(1)}+\Phi_a^{(2)}+\cdots$, and to iteratively obtain the solutions $\Phi^{(n)}$ from Eq. (8). Substituting the perturbative solutions into the definition (12), we obtain the nonlinear corrections to the power spectrum. This treatment is straightforward, but is plagued by a poor convergence of the perturbative expansion. Because of this, the applicable range of the standard perturbation theory (SPT) is restricted to a narrow range on large scales.

Recently, the improved treatment of the perturbation theory has been proposed by several authors employing the so-called renormalized/resummation techniques [7–13,20–22]. In these treatments, the naive expansion of the SPT is reorganized by introducing the nonperturbative statistical quantities, and the information of the higher-order corrections in SPT is effectively incorporated into each order of expansions. As a result, even truncating the expansion at some orders still contains the nonperturbative effects of nonlinear clustering, leading to the improvement of the convergence properties.

Here, among several nonperturbative techniques, we consider the closure theory proposed by Ref. [13], in which we have applied the nonlinear statistical method commonly used in the subject of turbulence (e.g., Ref. [15]) to the cosmological perturbation theory. In this treatment, the renormalized expansion has been first constructed according to the renormalized perturbation theory by Ref. [7]. Then, we truncate the expansions at the one-loop order. Under the tree-level approximation of the vertex function, this leads to a closed system of the power spectrum and nonlinear propagator. Though some nonperturbative properties are missed in this treatment, an advantage of this formulation is that we can compute the power spectrum numerically by solving the evolution equations, keeping full nonperturbative information of the nonlinear clustering at the one-loop order. This forward modeling may be suitable for a fast computation of the power spectrum, unlike the backward treatment of the perturbative expansions, which requires the time-consuming multidimensional integrations.

Let us define the nonlinear propagator, $G_{ab}(\boldsymbol{k}|\tau,\tau')$, and the cross-power spectra between different times, $R_{ab}(\boldsymbol{k};\tau,\tau')$:

$$\left\langle\frac{\delta\Phi_a(\boldsymbol{k},\tau)}{\delta\Phi_b(\boldsymbol{k}',\tau')}\right\rangle=G_{ab}(\boldsymbol{k}|\tau,\tau')\delta_D(\boldsymbol{k}-\boldsymbol{k}'), \quad (13)$$

$$\langle\Phi_a(\boldsymbol{k},\tau)\Phi_b(\boldsymbol{k}',\tau')\rangle=(2\pi)^3\delta_D(\boldsymbol{k}+\boldsymbol{k}')\times R_{ab}(|\boldsymbol{k}|;\tau,\tau');\quad(\tau>\tau'). \quad (14)$$

Then, the governing equations for power spectrum, equivalent to the renormalized expansions truncated at the one-loop level, become [13]

$$\hat{\Sigma}_{abcd}P_{cd}(k;\tau)=\int_{\tau_0}^{\tau}d\tau''M_{as}(k;\tau,\tau'')R_{bs}(k;\tau,\tau'')+\int_{\tau_0}^{\tau}d\tau''N_{a\ell}(k;\tau,\tau'')G_{b\ell}(k|\tau,\tau'')+(a\leftrightarrow b), \quad (15)$$

$$\hat{\Lambda}_{ab}R_{bc}(k;\tau,\tau')=\int_{\tau_0}^{\tau}d\tau''M_{as}(k;\tau,\tau'')R_{\overline{sc}}(k;\tau'',\tau')+\int_{\tau_0}^{\tau'}d\tau''N_{a\ell}(k;\tau,\tau'')G_{c\ell}(k|\tau',\tau''), \quad (16)$$

$$\hat{\Lambda}_{ab}G_{bc}(k|\tau,\tau')=\int_{\tau'}^{\tau}d\tau''M_{as}(k;\tau,\tau'')G_{sc}(k|\tau'',\tau'). \quad (17)$$

Here, $R_{\overline{sc}}(k;\tau'',\tau')=R_{sc}(k;\tau'',\tau')$ for $\tau''>\tau'$, $R_{cs}(k;\tau',\tau'')$ for $\tau''<\tau'$. The operator $\hat{\Sigma}_{abcd}$ is defined by

$$\hat{\Sigma}_{abcd}(\tau)=\delta_{ac}\delta_{bd}\frac{\partial}{\partial\tau}+\delta_{ac}\Omega_{bd}(\tau)+\delta_{bd}\Omega_{ac}(\tau). \quad (18)$$

The matrices M_{ab} and N_{ab} are

$$M_{as}(k;\tau,\tau'')=4\int\frac{d^3\boldsymbol{k}'}{(2\pi)^3}\gamma_{apq}(\boldsymbol{k}-\boldsymbol{k}',\boldsymbol{k}')\gamma_{\ell rs}(\boldsymbol{k}'-\boldsymbol{k},\boldsymbol{k})\times G_{q\ell}(k'|\tau,\tau'')R_{pr}(|\boldsymbol{k}-\boldsymbol{k}'|;\tau,\tau''), \quad (19)$$

$$N_{a\ell}(k;\tau,\tau'') = 2\int \frac{d^3\boldsymbol{k}'}{(2\pi)^3}\gamma_{apq}(\boldsymbol{k}-\boldsymbol{k}',\boldsymbol{k}')\gamma_{\ell rs}(\boldsymbol{k}-\boldsymbol{k}',\boldsymbol{k}') \times R_{qs}(k';\tau,\tau'')R_{pr}(|\boldsymbol{k}-\boldsymbol{k}'|;\tau,\tau''). \quad (20)$$

Note that we have recast the original equations in Ref. [13] in more symmetrical way by changing the integration variable [c.f. Eqs. (49)–(53) of Ref. [13]]. By definition, the nonlinear propagator and the cross-power spectra should satisfy the boundary condition:

$$G_{ab}(k|\tau,\tau) = \delta_{ab}, \quad (21)$$

$$\lim_{\tau'\to\tau} R_{ab}(k;\tau,\tau') = P_{ab}(k;\tau). \quad (22)$$

The closure Eqs. (15)–(17) are the integro-differential equations involving several nonlinear terms, in which the information of the higher-order correction in SPT is encoded. Thus, replacing the statistical quantities R_{ab} and G_{ab} in nonlinear terms with linear-order ones, the solutions of closure equations automatically reproduce the leading-order results of SPT, i.e., one-loop power spectra. Here, the linear-order quantities denoted by $R^{\rm L}_{ab}$ and $G^{\rm L}_{ab}$ satisfy

$$\hat{\Lambda}_{ab}G^{\rm L}_{bc}(k|\tau,\tau') = 0, \quad (23)$$

$$\hat{\Lambda}_{ab}R^{\rm L}_{bc}(k;\tau,\tau') = 0; \qquad (\tau>\tau'). \quad (24)$$

For the rest of this paper, we focus on the numerical treatment of the closure equations and demonstrate the evolution of matter power spectrum in both nonlinear and quasilinear regimes by changing the treatment of nonlinear terms.

IV. NUMERICAL METHOD

The closure Eqs. (15)–(17) are the nonlinear coupled equations involving the time-consuming integrals over space and time. In order to numerically treat these messy integrals while keeping computational cost, we implement the method used by Ref. [9], in which the propagator and power spectra are expanded by a set of basis functions of k, and integrated with respect to k in advance of the time evolution. We adopt the trapezoidal rule for the integration with respect to τ and k, and the central difference formula for the time evolution. To be precise, we first prepare a discretized set of k labeled as k_m for $m = 1,\cdots,N_k$, where we denote k_1 and k_{N_k} by $k_{\rm min}$ and $k_{\rm max}$, respectively. We define a set of triangular-shaped functions as the basis functions:

$$\mathcal{T}_m(k) = \begin{cases} \frac{k-k_{m-1}}{k_m-k_{m-1}}; & k_{m-1}\le k<k_m, \\ \frac{k_{m+1}-k}{k_{m+1}-k_m}; & k_m\le k<k_{m+1}, \\ 0; & \text{otherwise.}\end{cases} \quad (25)$$

Then we expand the nonlinear propagator, the auto- and cross-power spectra as

$$P_{ab}(k';\tau) = \sum_m \mathcal{P}_{ab,m}(\tau)\mathcal{T}_m(k'), \quad (26)$$

$$R_{ab}(k';\tau',\tau) = \sum_m \mathcal{R}_{ab,m}(\tau',\tau)\mathcal{T}_m(k'), \quad (27)$$

$$G_{ab}(k'|\tau',\tau) = \sum_m \mathcal{G}_{ab,m}(\tau',\tau)\mathcal{T}_m(k'). \quad (28)$$

The above expressions together with basis function (25) imply that the power spectra and the propagator between the discrete points are evaluated by the linear interpolation according to the definition of the basis functions. Note that these functions do not satisfy the orthogonality in the sense that the integration of the product $\mathcal{T}_m(k)\mathcal{T}_n(k)$ over the continuous space of k does not vanish even if $m \neq n = m+1$. The set of $\mathcal{T}_m(k)$ has the orthogonality only on the discrete space because $\mathcal{T}_m(k_i) = \delta_{mi}$ is satisfied.

Substituting Eqs. (26)–(28) into Eqs. (19) and (20), we obtain a separable form of the matrices M_{ab} and N_{ab} :

$$M_{as}(k;\tau,\tau'') = \sum_{\text{all indices}} \mathcal{G}_{q\ell,m}(\tau,\tau'')\mathcal{R}_{pr,n}(\tau,\tau'') \times \mathcal{T}^{(M)}_{apq,\ell rs,m,n}(k), \quad (29)$$

$$N_{a\ell}(k;\tau,\tau'') = \sum_{\text{all indices}} \mathcal{R}_{qs,m}(\tau,\tau'')\mathcal{R}_{pr,n}(\tau,\tau'') \times \mathcal{T}^{(N)}_{apq,\ell rs,m,n}(k), \quad (30)$$

where $\mathcal{T}^{(M)}$ and $\mathcal{T}^{(N)}$ are given by

$$\mathcal{T}^{(M)}_{apq,\ell rs,m,n}(k) = 4\int \frac{d^3\boldsymbol{k}'}{(2\pi)^3}\gamma_{apq}(\boldsymbol{k}-\boldsymbol{k}',\boldsymbol{k}')\gamma_{\ell rs}(\boldsymbol{k}'-\boldsymbol{k},\boldsymbol{k}) \times \mathcal{T}_m(k')\mathcal{T}_n(k-k'), \quad (31)$$

$$\mathcal{T}^{(N)}_{apq,\ell rs,m,n}(k) = 2\int \frac{d^3\boldsymbol{k}'}{(2\pi)^3}\gamma_{apq}(\boldsymbol{k}-\boldsymbol{k}',\boldsymbol{k}')\gamma_{\ell rs}(\boldsymbol{k}-\boldsymbol{k}',\boldsymbol{k}') \times \mathcal{T}_m(k')\mathcal{T}_n(k-k'). \quad (32)$$

The details of the description on the integrations (31) and (32) can be found in Appendix A. Although Eqs. (31) and (32) seem to have many components, most of them vanishes because the vertex function γ_{abc} has only three non-vanishing components given in Eq. (9). The relevant components in the summation are listed in Table I.

Based on the essential points of our numerical treatment described above, we now consider how to solve the closure equations in a cosmological setup. Basically, we perform the following steps (see also Fig. 1):

(1) Set $\tau = \tau_{\rm init}$ (or $z = z_{\rm init}$) for sufficiently small value of $\tau_{\rm init} < 0$, where the universe is well-described by the Einstein-de Sitter (EdS) model, and impose the initial conditions:

TABLE I. List of nonvanishing components of the function $\mathcal{T}^{(M,N)}_{apq,\ell rs,m,n}(k)$ in Eqs. (29) and (30).

(a, s)	$(apq, \ell rs)$ for M
(1, 1)	(112, 121), (121, 121)
(1, 2)	(112, 112), (112, 222), (121, 112), (121, 222)
(2, 1)	(222, 121)
(2, 2)	(222, 112), (222, 222)
(a, ℓ)	$(apq, \ell rs)$ for N
(1, 1)	(112, 112), (112, 121), (121, 112), (121, 121)
(1, 2)	(112, 222), (121, 222)
(2, 1)	(222, 112), (222, 121)
(2, 2)	(222, 222)

$$P_{ab}(k;\tau_{\rm init}) = R_{ab}(k;\tau_{\rm init},\tau_{\rm init}) = \begin{pmatrix} 1 & 1 \\ 1 & 1 \end{pmatrix} P_{\rm init}(k),$$
$$G_{ab}(k|\tau_{\rm init},\tau_{\rm init}) = \delta_{ab}, \qquad (33)$$

where $P_{\rm init}(k)$ is the linear power spectrum given at the initial time $\tau_{\rm init}$. Note that, in order to ensure the validity of this prescription, the initial condition should be imposed early enough so that the influences of the nonlinearity and the transient from the initial condition can be neglected. Appropriate value of the initial time has been chosen based on the convergence test in Appendix B.

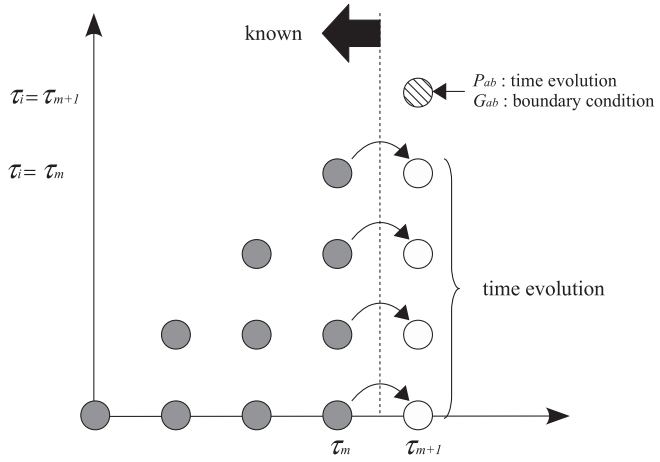

FIG. 1. Schematic draw of the numerical procedure to solve closure equations. Each circle represents both $\mathcal{G}_{ab,p}$ and $\mathcal{R}_{ab,p}$ ($\mathcal{P}_{ab,p}$ for $\tau_i = \tau_m$) on the discrete time grid, just omitting the wave number dependence. The horizontal and vertical axes correspond to the second and third arguments of those quantities. In the steps 3 and 4 mentioned in the main text, we compute the matrices $M_{ab}(k;\tau_m,\tau_i)$ and $N_{ab}(k;\tau_m,\tau_i)$ for $0 \le i \le m$, and evaluate the nonlinear terms, depicted as filled circles at the right edge of the 'known' region. In next step 5, we advance the time step and obtain $\mathcal{G}_{ab,p}(\tau_{m+1},\tau_i)$ and $\mathcal{R}_{ab,p}(\tau_{m+1},\tau_i)$ for $0 \le i \le m$ (blank circles), and $\mathcal{P}_{ab,p}$ and $\mathcal{G}_{ab,p}$ for $(\tau_{m+1}, \tau_b m+1)$ (shaded circle).

(2) Perform the integration over k for all components of $\mathcal{T}^{(M)}_{apq,\ell rs,m,n}$ and $\mathcal{T}^{(N)}_{apq,\ell rs,m,n}$ using the trapezoidal rule [see Eqs. (31) and (32)].
(3) Suppose that the coefficients $\mathcal{G}_{ab,p}(\tau_m,\tau_i)$ and $\mathcal{R}_{ab,p}(\tau_m,\tau_i)$ for $0 \le i \le m$ have been already obtained (filled circles in Fig. 1), we perform the summation in Eqs. (29) and (30), and compute the kernels $M_{ab}(k;\tau_m,\tau_i)$ and $N_{ab}(k;\tau_m,\tau_i)$.
(4) Calculate the nonlinear terms in the right-hand side of Eqs. (15)–(17). We use the trapezoidal rule for the integration over time τ''.
(5) Advance the time step from τ_m to τ_{m+1}, and obtain a new set of arrays $G_{ab}(k|\tau_{m+1},\tau_i)$, $R_{ab}(k;\tau_{m+1},\tau_i)$ and $P_{ab}(k;\tau_{m+1})$ for $0 \le i \le m$, applying the central difference formula to Eqs. (15)–(17) (open circles in Fig. 1). For the edge of arrays (shaded circle in Fig. 1), the boundary conditions (21) and (22) are used to obtain $G_{ab}(k|\tau_{m+1},\tau_{m+1})$ and $R_{ab}(k;\tau_{m+1},\tau_{m+1})$.
(6) Repeat the steps 3–5 until the time τ_{n+1} reaches the final time.

Note that the trapezoidal rule at step 4 and finite difference scheme at steps 5 are explicitly written as follows. For Eq. (17) with $(\tau,\tau') = (\tau_p,\tau_q)$, we have

$$\frac{\mathcal{G}_{ab,r}(\tau_{p+1},\tau_q) - \mathcal{G}_{ab,r}(\tau_{p-1},\tau_q)}{2\Delta\tau} + \Omega_{ab}(\tau_p)\mathcal{G}_{bc,r}(\tau_p,\tau_q)$$
$$= \Delta\tau \sum_{m=q}^{p} c_m M_{as}(k_r;\tau_p,\tau_m)\mathcal{G}_{sc,r}(\tau_m,\tau_q), \qquad (34)$$

for $p > q$. In cases with $p = q$, the differentiation in left-hand side of the above equation is replaced with the first-order difference. Here, we set $c_m = 1/2$ for $m = q,\ p$, otherwise $c_m = 1$. Equations (15) and (16) can be also written similarly as above.

The above procedure can be also used for the calculation of the one-loop spectra in SPT. As we mentioned in Sec. III, the calculation in the SPT additionally needs the solutions $G^{\rm L}_{ab}$ and $R^{\rm L}_{ab}$ given in Eqs. (23) and (24) in advance. They are used at the step 3 to compute the integration kernels, $M^{\rm L}_{ab}$ and $N^{\rm L}_{ab}$, which are evaluated from Eqs. (19) and (20) just replacing the integrands with linear-order ones. In the same manner, at the step 4, we replace G_{ab} and R_{ab} in the nonlinear interaction terms with linear-order quantities, $G^{\rm L}_{ab}$ and $R^{\rm L}_{ab}$, respectively.

V. DEMONSTRATIONS

In what follows, we present the results of numerical integration of closure equations. We first demonstrate the full nonlinear calculation and present the results in Sec. V A. Then, we move to discuss the perturbative treatment and examine the weakly nonlinear evolution of the power spectrum in dark energy and modified gravity models in Sec. V B. The initial power spectrum $P_{\rm init}(k)$ is

calculated from the linear transfer function in the flat ΛCDM model. We adopt the cosmological parameters determined from WMAP five-year results [6]: $\Delta^2_{\mathcal{R}}(k_0 = 0.002\ \mathrm{Mpc}^{-1}) = 2.457 \times 10^{-9}$, $n_s = 0.960$, $\Omega_{\mathrm{m}} = 0.279$, $h = 0.701$, for the amplitude of curvature perturbation, scalar spectral index, density parameter of matter, and Hubble parameter, respectively. Unless otherwise stated, we assume the dark energy with equation-of-state parameter $w_{\mathrm{de}} = -1$.

The parameters of our numerical calculations include the initial redshift z_{init}, the cutoff wave number k_{max}, the number of time steps N_τ, and the number of Fourier mesh N_k. We set $N_\tau = 172$ and $N_k = 200$ with constant interval in linear and logarithmic scales, respectively. For the initial redshift and cutoff wave number, based on the convergence test in Appendix B, we chose $z_{\mathrm{init}} = 200$ and $k_{\mathrm{max}} = 5h\ \mathrm{Mpc}^{-1}$. With this choice, the numerical errors in the SPT calculation are reduced to a sub-percent level.

A. Full nonlinear calculation

In the full nonlinear treatment, the solutions of auto- and cross-power spectra as well as the nonlinear propagator are simultaneously obtained from the closure equations at each time step. Here, for illustrative purpose, we first show the nonlinear propagators, which clearly manifest the nonperturbative property of nonlinear clustering incorporated into our formalism.

Figure 2 plots the nonlinear propagator $G_{11}(k|z, z_{\mathrm{init}})$ as function of wave number given at different redshifts, $z =$ 0.5, 2 and 5 (from left to right). Clearly, the numerical results depicted as solid lines exhibit the damping oscillation, and asymptotically approach zero at $k \to \infty$. The characteristic scale of the damping is shifted to a lower k for decreasing the redshift. These behaviors are marked contrast with the linear theory prediction depicted as dotted line. Note that the results including the leading-order correction (one-loop SPT) slightly improves the low-k behavior, but they eventually become negative and diverge at $k \to \infty$. In this respect, the damping properties seen in the numerical results can be regarded as the nonperturbative effect, which results from the resummation of infinite series of higher-order corrections. Indeed, the damping behavior in the nonlinear propagators has been already confirmed in the N-body simulations [8,23], and is essential for the accurate prediction of power spectrum [12].

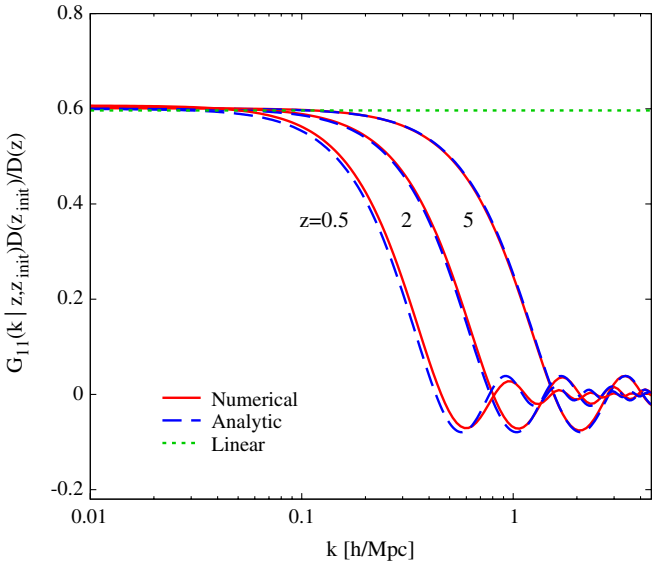

FIG. 2 (color online). The nonlinear propagators $G_{11}(k|z, z_{\mathrm{init}})$ at $z = 0.5$, 2, and 3 from left to right. The vertical axis is normalized by the linear growth rate, $D(z)$. The solid lines represent the numerical solution of the closure Eqs. (15)–(17). The dashed line are the approximate solution derived in Ref. [13], and the dotted line indicates the linear theory prediction.

In Fig. 2, the dashed lines indicate the analytic results obtained from Ref. [13]. Basically, these are the approximate solutions of Eq. (17) constructed by matching the asymptotic solutions in the low-k and high-k limits. Although the analytic results at lower redshifts slightly deviate from the numerical solutions, the overall agreement between these two curves is remarkable. This may be an independent check for the stability of our numerical scheme, and the accuracy of our code seems comparable to or even better than the analytic calculations.

Now, in Fig. 3, we show the redshift evolution of the matter power spectrum, $P_{11}(k; z)$, obtained from the closure equations. For comparison, we also plot the N-body results taken from Ref. [17]. Solid lines represents the numerical results of closure equations, dashed and dotted lines are the results of analytic calculations including up to the leading-order and next-to-leading order perturbative corrections, respectively. Here, the analytic results were obtained based on the integral solutions of the closure equations presented in Ref. [13,17]. We employ the Born approximation to evaluate the integral solutions perturbatively. Although the analytical treatment is found to accurately describe the nonlinear evolution of baryon acoustic oscillations with a precision of sub-percent level [16,17], because of the perturbative treatment, applicable range of the analytic treatment is limited to a narrow range. As clearly shown in Fig. 3, the resultant power spectra rapidly fall off at some higher wave numbers. By contrast, the power spectra obtained from the numerical calculation first trace the analytical results on large scales, and they extend over small scales without a sharp drop of the amplitude. Remarkably, the numerical results quite resemble the N-body results at $k \lesssim 1(0.6)h\ \mathrm{Mpc}^{-1}$ for $z = 3$ ($z = 0.5$), and the agreement between these two results reaches the accuracy of ~4%(8%) level. This is a clear manifestation of the fact that full nonlinear treatment of the closure equations is indeed a nonperturbative way of calculating the power spectrum beyond the weakly nonlinear regime. Hopefully, it would be a fast computational tool comple-

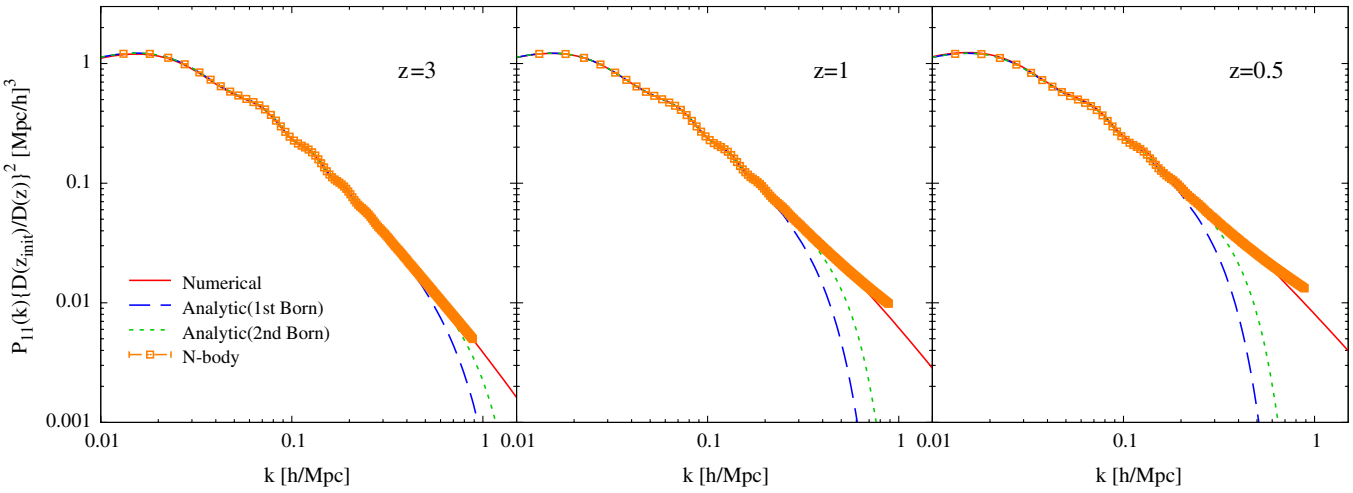

FIG. 3 (color online). Time evolution of matter power spectra, $P_{11}(k)$, evaluated at $z = 3$, 1 and 0.5 from left to right panels. The vertical axis is normalized by the linear growth rate, $D(z)$. The solid lines represent the numerical solution of the Eqs. (15)–(17). The dashed and dotted lines are the analytic results including the corrections up to the first- and second-order Born approximation, respectively [13]. The squares with error bars indicate the N-body simulations taken from Ref. [17].

mentary to the N-body simulations. To clarify the usefulness of this approach, a more quantitative comparison between N-body simulations and our numerical treatment is needed. We will discuss this issue in a future work.

B. Perturbative calculation

In this subsection, we turn to focus on the perturbative treatment of the closure equations, by which all the quantities in nonlinear terms are replaced with the linear-order ones. As we mentioned, this treatment automatically reproduces the one-loop results of SPT. Owing to the numerical treatment, we can address weakly nonlinear evolution even when the analytical calculations are no longer possible. In Sec. V B 1, we discuss the one-loop power spectra in dark energy models, and address the validity of the analytical treatment based on the Einstein-de Sitter approximation. In Sec. V B 2, we examine a class of modified gravity models with linear Poisson equation, where the effective Newton constant manifestly depends on scale. We demonstrate how the modification of the gravitational-force law affects the power spectra in weakly nonlinear regime.

1. Dark energy models

The one-loop SPT has recently attracted renewed interest for an accurate modeling of large-scale structure. In particular, a precise measurement of baryon acoustic oscillations made by ongoing and/or upcoming galaxy surveys to probe the nature of late-time cosmic acceleration provide a strong motivation to use the one-loop SPT for an accurate template of matter power spectrum (e.g., Refs. [16,24–26]). In these experiments, the required accuracy for theoretical template reaches at a percent level.

In the analytic treatment of one-loop power spectra, the Einstein-de Sitter (EdS) approximation has been frequently used in the literature (e.g., Ref. [14] and references therein). Under the approximation, the higher-order solutions of perturbation are approximately described by the linear growth factor $D(z)$, and the resultant power spectra are schematically expressed as

$$P_{ab}(k;z) = D^2(z)P^{\rm L}_{ab}(k) + D^4(z)P^{1-{\rm loop}}_{ab}(k) + \cdots. \quad (35)$$

Note that for dark energy models in general relativity, the EdS approximation is mathematically equivalent to solving the closure equations just replacing the matrix Ω_{ab} in the operators $\hat{\Lambda}_{ab}$ and $\hat{\Sigma}_{abcd}$ with

$$\Omega^{\rm EdS}_{ab}(\tau) = \begin{pmatrix} 0 & -1 \\ -\frac{3}{2}f^2 & \frac{f}{2} - \frac{d\ln f}{d\tau} \end{pmatrix}, \quad (36)$$

with the function f defined by $f \equiv d\ln D/d\tau$.

Here, we consider two specific examples of dark energy models characterized by the equation-of-state parameter $w_{\rm de}$ as [27,28]

$$w_{\rm de}(a) = w_0 + w_a(1-a), \quad (37)$$

and [29]

$$w_{\rm de}(a) = w_0 w_1 \left(\frac{a^q + a_s^q}{w_1 a^q + w_0 a_s^q} \right). \quad (38)$$

Comparing the numerical results of closure equations with the analytical calculations, we discuss the validity of EdS approximation.

Figure 4 shows the one-loop spectra $P_{11}(k)$ (*left*) and $P_{22}(k)$ (*right*) at $z = 0.5$ and 3, for dark energy model with slowly varying $w_{\rm de}$ [Eq. (37)]. The model parameters w_0 and w_a were appropriately chosen within the currently

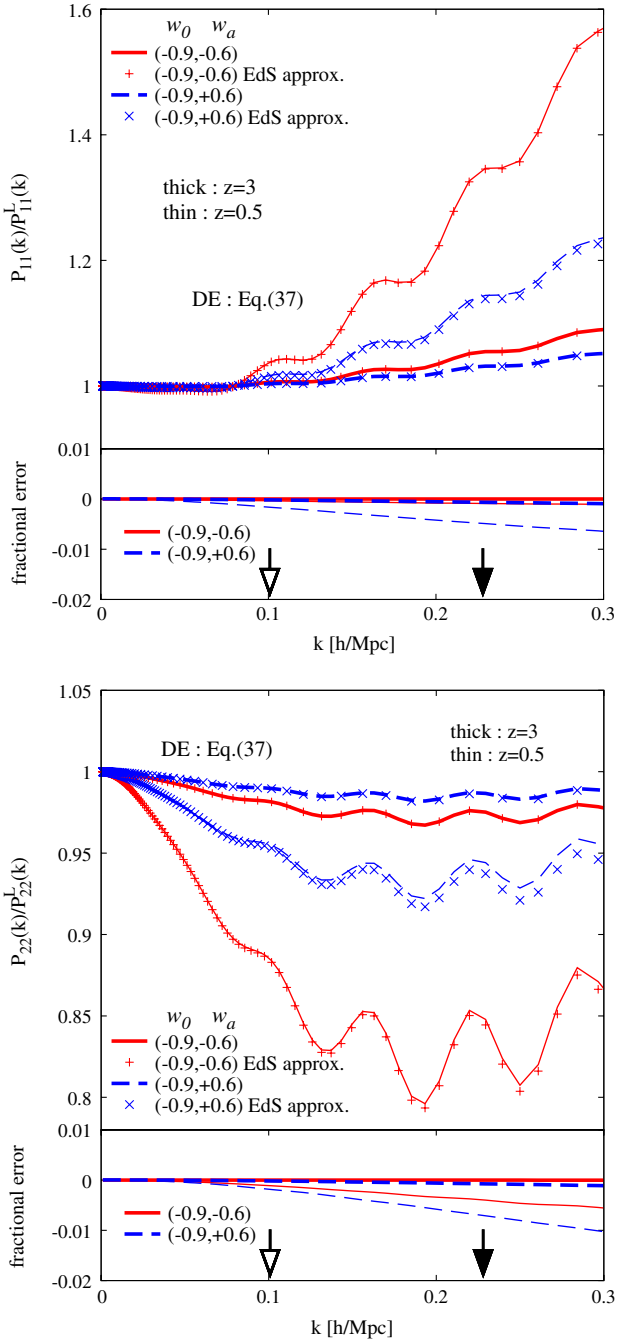

FIG. 4 (color online). The density (*left*) and velocity-divergence power spectra (*right*) normalized by the linear theory predictions in dark energy model with variable $w_{\rm de}$ [see Eq. (37)]. The symbols and lines, respectively, represent the results with and without the EdS approximation: $(w_0, w_a) = (-0.9, -0.6)$ (solid lines and symbol '+'); $(-0.9, +0.6)$ (dashed lines and symbol '×'). In bottom panels, the differences between these results are plotted as the fractional error, $\{P^{(\rm EdS)}(k) - P^{(\rm num)}(k)\}/P^{(\rm num)}(k)$. The thick (thin) lines are the results at $z = 3(0.5)$. The vertical arrows indicate the maximum wave number below which the prediction of SPT is expected to agree well with the N-body simulations within 1% (see Eq. (39), and Ref. [16]). The filled and open arrows are the maximum wave numbers at $z = 3$ and $z = 0.5$, respectively.

constrained values of $|1 + w_0| \lesssim 0.1$ and $|w_a| \lesssim 0.6$ (e.g., Ref. [6]). In upper panels, we plot the ratio of power spectra, $P_{ab}(k)/P^{\rm L}_{ab}(k)$, while in lower panels, we plot the fractional difference between the results with and without EdS approximation, i.e., $\{P^{(\rm EdS)}(k) - P^{(\rm num)}(k)\}/P^{(\rm num)}(k)$, where $P^{(\rm EdS)}$ and $P^{(\rm num)}$ are, respectively, obtained from the analytic and numerical calculations. Similarly, in Fig. 5, we plot the results in the dark energy model (38), in which the equation-of-state parameter has a sharp transition from w_1 to w_0 at the scale factor $a \sim a_s$ for a large q.

The resultant power spectra with EdS approximation underestimate the numerical results without EdS approximation in both the density and velocity-divergence part of autopower spectra. As decreasing the redshift, the deviation from numerical results becomes significant, but a level of discrepancy is not so large. These are consistent with the previous findings by Refs. [22,30], from the analysis of matter power spectrum. In Figs. 4 and 5, the vertical arrows indicate the maximum wave number below which the precision level of one-loop SPT is expected to be better than 1%. According to Ref. [16], this is determined by solving the following equation with respect to the wave number k:

$$\frac{k^2}{6\pi^2}\int_0^k P^{\rm L}_{11}(q;z)dq = 0.18. \tag{39}$$

Note that the maximum wave numbers given above have been empirically derived by comparison between N-body simulations and theoretical predictions, and it seems rather conservative estimates compared to those previously proposed [11,24,31]. Keeping the limitation of the one-loop SPT in mind, we confirm that the analytical treatment with EdS approximation is a quite good description of the one-loop power spectra and the accuracy of this treatment can reach a sub-percent level. This is even true for the model (38) with the extreme parameter set, i.e., $(w_0, w_1, a_s, q) = (-1.8, -0.4, 0.5, 25.0)$, in which the effective equation-of-state parameter $w_{\rm eff} \equiv -1 - (2/3)d\ln H/d\tau$, rather than $w_{\rm de}$, sharply changes its sign at $a \sim 0.5$ and eventually approaches $w_{\rm eff} \sim 1$.

Therefore, as long as the dark energy models in general relatively are concerned, the analytical calculation with EdS approximation is very accurate treatment within the validity range of predictions, and it can give a fast computation of the weakly nonlinear power spectrum.

2. Modified gravity models

Now let us consider the weakly nonlinear evolution of the power spectrum in modified gravity models with linear Poisson equation. Unlike the dark energy models, the Newton constant is effectively modified, and even the linear growth rate generically depends on the scale and time. Thus, the EdS approximation cannot be applied in

general and the analytical treatment is no longer possible.[1] Here, we demonstrate that with the use of the present formalism and numerical method, the one-loop power spectrum can be accurately computed even in the analytically intractable cases.

We examine two representative modified gravity models whose effective Newton constant manifestly depends on the scale and time. One is a phenomenological model in which the Yukawa interaction is added by hand to the inverse-square law (e.g., Refs. [32–34]). The effective Newton constant in this model is given by

$$G_{\rm eff}(k,\tau) = G\left\{1 + \alpha\frac{1}{\lambda^2(k/a)^2 + 1}\right\}. \qquad (40)$$

The parameter λ is the characteristic (proper) length at which the Newton force is modified, and the amplitude α represents the strength of the deviation from the inverse-square law on large scales. Note that cosmological constraints on these parameters have been obtained recently from the galaxy power spectrum of the Sloan Digital Sky Survey [33,34]. Based on this, we compute the power spectra for specific parameters with $(\lambda, \alpha) = (20h^{-1}\text{Mpc}, 1)$ and $(100h^{-1}\text{ Mpc}, 1)$.

As another example, we consider the $f(R)$ gravity model. This model has been recently attracted as one of the successful models that explains late-time cosmic acceleration [35–37] (and see also Ref. [4] for a review). The $f(R)$ gravity model is given by the generalization of the Einstein-Hilbert action to include arbitrary function of the scalar curvature R:

$$S = \int d^4x\sqrt{-g}\left[\frac{R + f(R)}{16\pi G} + \mathcal{L}_{\rm m}\right], \qquad (41)$$

with $\mathcal{L}_{\rm m}$ being the Lagrangian of ordinary matter. Under the quasistatic treatment relevant for the scales well-inside the Hubble horizon, the effective Newton constant becomes (e.g., Ref. [38])

$$G_{\rm eff}(k,\tau) = G\left\{\frac{4}{3} - \frac{1}{3}\frac{\bar{\mu}^2}{(k/a)^2 + \bar{\mu}^2}\right\}, \qquad (42)$$

where the quantity $\bar{\mu}^2$ is the effective mass of the new scalar degree of freedom, f_R, and is defined by $\bar{\mu}^2 = \{(1 + f_R)/(\partial f_R/\partial R) - R\}/3$. Note that the barred quantity $\bar{\mu}^2$ implies the one evaluated in terms of the background quantities. In general, the corrections coming from nonlinear interaction terms appear in $G_{\rm eff}$, but we do not consider here. In the present paper, we specifically consider the function $f(R)$ of the form, $f(R) \propto R/(AR + 1)$ [35,38–40]. In the cosmologically interesting setup with $R \to 0$ and $f(R) \to 0$, this can be expanded as

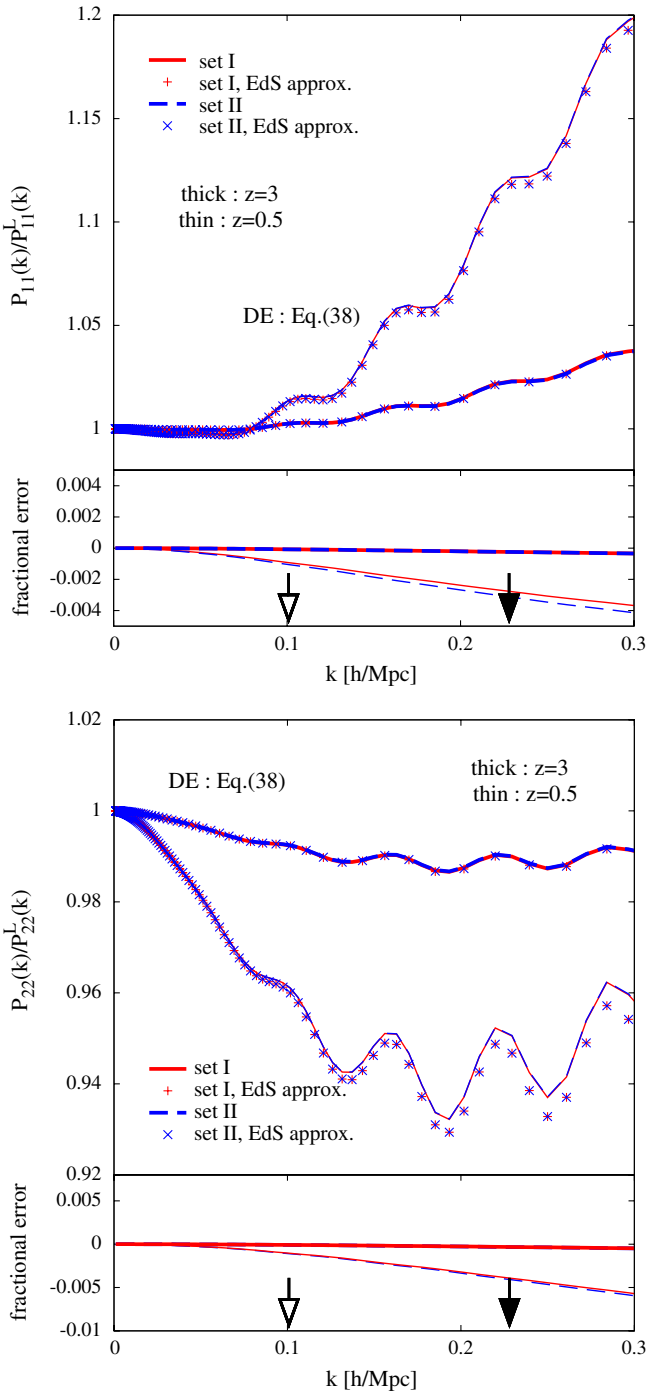

FIG. 5 (color online). Same as in Fig. 4, but in the dark energy model with equation-of-state parameter (38). The model parameters are set to $(w_0, w_1, a_s, q) = (-1.8, -0.4, 0.5, 3.41)$ for *set I*, and $(-1.8, -0.4, 0.5, 25.0)$ for *set II*. Note that the case with parameters of *set II* is regarded as extreme one, in which the effective equation-of-state parameter, $w_{\rm eff} \equiv -1 - (2/3)d\ln H/d\tau$, sharply changes its sign at $a \sim 0.5$. As for the vertical arrows, see the caption of Fig. 4.

[1] In the DGP model as one of the successful models that explains the late-time cosmic acceleration [3], the effective Newton constant $G_{\rm eff}$ depends only on time at the linear-order level, and the analytical calculation of one-loop spectrum is possible with a help of EdS approximation, even in the presence of nonlinearity in Poisson equation [18].

$$f(R) \simeq -16\pi G\rho_\Lambda - f_{R0}\left(\frac{\bar{R}_0}{R}\right). \tag{43}$$

The energy density ρ_Λ is related with the constant A, and $\bar{R}_0$ and f_{R0} are the background curvature and the field value given by $f_R(R_0)$ at present time. Here, we consider the cases with $|f_{R0}| \ll 1$, in which the last term at the right-hand side of Eq. (43) is safely negligible and the background expansion just follows the same expansion history as in the ΛCDM model.

Figure 6 shows the numerical results of one-loop power spectra given at $z = 0.5$. Left and right panels plot the results for the models with effective Newton constant (40) and (42), respectively. The upper panels show the ratio of matter power spectrum, $P_{11}(k)/P^{\rm L}_{11}(k)$, while in lower panels, the fractional enhancement relative to the ΛCDM model, i.e., $\{P(k) - P_{\Lambda\rm CDM}(k)\}/P_{\Lambda\rm CDM}(k)$, is plotted. In model with Eq. (40), the modification of the gravitational-force law appears on large scales, and the effective Newton constant becomes $G_{\rm eff} \to (1 + \alpha)G$. On the other hand, the Newton constant on small scales becomes $4/3$ times greater than that on large scales in the model with Eq. (42). This scale-dependent nature qualitatively explains the results seen in the lower panels, and because of this, the resultant shape of the one-loop spectra is significantly altered. Nevertheless, when normalized by the linear power spectra, which intrinsically possesses the scale-dependent nature of $G_{\rm eff}$ through the linear growth rate, the differences in the mode transfer efficiency between two models turn out to be small (see upper panel). This indicates that the modification of gravitational-force law imprinted in the linear power spectrum can be preserved in the weakly nonlinear regime, and the linear growth rate becomes an important clue to distinguish between various modified gravity models. This would be even true for a large class of the modified gravity models with nonlinear Poisson equation.

Finally, it is interesting to note that in the model with Eq. (42), there appears the crossing point at which the dependence of the ratio $P(k)/P^{\rm L}(k)$ on $|f_{R0}|$ is changed. As shown in the upper-right panel, the ratio decreases with $|f_{R0}|$ on large scales, while it eventually increases on small scales. This behavior basically reflects the fact that the strong gravity on small scales efficiently promotes the mode transfer from the low-k to high-k modes.

VI. DISCUSSION AND CONCLUSION

In this paper, on the basis of the nonperturbative framework of the cosmological perturbation theory developed by Ref. [13], we have presented a numerical scheme to treat nonlinear evolution of matter power spectrum. The governing equations for matter power spectra are a closed set of evolution equations coupled with nonlinear propagator, which has been previously derived by truncating the infinite chain of moment equations, with a help of perturbative calculation called closure approximation. The present formulation is equivalent to the one-loop level of renormalized perturbation theory, and the nonperturbative effects of gravitational clustering are effectively incorporated into the solution of closure equations. Note that the closure equations consistently reproduces the so-called one-loop

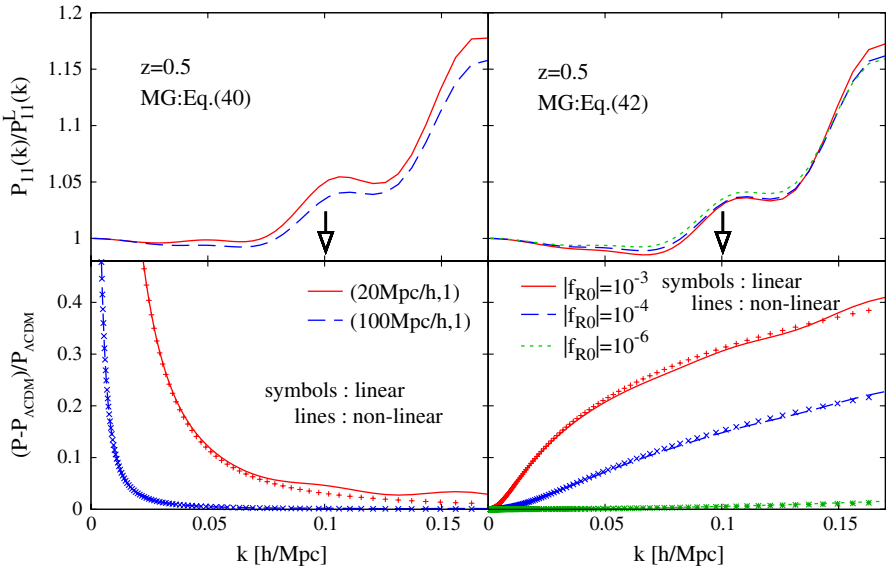

FIG. 6 (color online). Weakly nonlinear power spectrum at $z = 0.5$ in a modified gravity model with Yukawa-type interaction (*left*) and $f(R)$ gravity model (*right*). The symbols, '+', '×' and '*', respectively, represent the resultant spectra in the linear theory, and lines the nonlinear numerical solutions. The upper panels show the power spectra divided by the linear ones, and the lower ones indicate the deviations from the spectra calculated in the flat ΛCDM model. Note that the symbols in lower panels represent the linear theory predictions.

results of standard perturbation theory if we replace the quantities in the nonlinear terms with linear-order ones. The numerical scheme presented here can be used for the predictions of matter power spectra in both quasi nonlinear and nonlinear regimes, and is applicable to the analytically intractable cases. The modification to the gravity sector is straightforward.

We have demonstrated that the full nonlinear treatment of the closure equations has a ability to treat nonlinear evolution of power spectrum beyond the validity regime of previous analytical calculations. The resultant shape of the nonlinear spectrum resembles the N-body result, and the agreement between these two results reaches the accuracy of $\sim 4\%(8\%)$ level at $z = 3(z = 0.5)$. We then focused on the perturbative treatment of closure equations, and presented the numerical results of one-loop SPT in various situations. We discussed the validity of the analytical treatment based on the Einstein-de Sitter approximation which has been frequently used in the literature. In the dark energy models with two representative equation-of-state parameters (37) and (38), we found that the analytical calculation with Einstein-de Sitter approximation provides an excellent description for the density and velocity-divergence components of the one-loop power spectrum. Within the validity range of one-loop spectra, the accuracy of this treatment reaches at a sub-percent level. Also, we have studied the one-loop power spectra in a class of modified gravity models, in which the effective Newton constant manifestly depends on the scale and time, and the analytical calculation is no longer possible. We demonstrated that the scale-dependent modification of the gravitational-force law alters the power spectrum significantly, but the efficiency of the mode transfer arising from the nonlinear mode coupling changes only moderately. In this respect, the modification of the gravity imprinted in the linear power spectrum would be preserved in the weakly nonlinear regime, and the (scale-dependent) linear growth rate may be an important clue to distinguish between various modified gravity models.

The numerical scheme presented here is a first step toward precisely modeling the nonlinear evolution of matter power spectrum in various situations. Recently, the nonlinear spectrum including the massive neutrinos has been investigated by Ref. [41] based on the approach similar to our formalism [22]. Incorporating the effect of massive neutrinos into the present formalism is rather straightforward, and the closure equations may be used for a nonperturbative calculation of matter power spectrum beyond the free-streaming scales. As another direction, one may consider the extension of the present formulation to deal with a wide class of modified gravity models with nonlinear Poisson equation. Ref. [18] presented a general formalism to treat such models and explicitly calculated the one-loop power spectrum in DGP and $f(R)$ gravity models from the closure equations. The results for full nonlinear treatment are left for future work, and will be reported elsewhere.

ACKNOWLEDGMENTS

We would like to thank Takahiro Nishimichi for providing us the numerical data of his N-body simulations. A. T. is supported by a Grant-in-Aid for Scientific Research from the Japan Society for the Promotion of Science (JSPS) (No. 18740132). This work was supported in part by Grant-in-Aid for Scientific Research on Priority Areas No. 467 "Probing the Dark Energy through an Extremely Wide and Deep Survey with Subaru Telescope", and JSPS Core-to-Core Program "International Research Network for Dark Energy".

APPENDIX A: DETAILS OF NUMERICAL INTEGRATIONS IN EQS. (31) AND (32)

In this appendix, we discuss the technical details on the numerical integrations of the nonlinear terms in closure equations. In the numerical algorithm presented in Sec. IV, we must evaluate Eqs. (31) and (32) in advance to the time evolution. To compute these integrals, the expressions are first rewritten with the form of the two-dimensional integral with a help of the symmetry in the integrands. Then, we introduce the elliptic coordinate used in Ref. [9], and perform the integration by the trapezoidal rule taking carefully account of the domain of integration.

The elliptic coordinate is defined as

$$\boldsymbol{k}' = \frac{\boldsymbol{k}}{2} + \mathbf{q}, \qquad \mathbf{q} = \frac{k}{2}\begin{pmatrix} \sinh\zeta \sin\mu \cos\phi \\ \sinh\zeta \sin\mu \sin\phi \\ \cosh\zeta \cos\mu \end{pmatrix}, \tag{A1}$$

where the vector $\boldsymbol{k}$ is set to be aligned to the third axis. We introduce

$$X = \cosh\zeta, \qquad Y = \cos\mu, \tag{A2}$$

where $X \geq 1$ and $-1 \leq Y \leq 1$. In Fig. 7, we schematically plot the elliptic coordinate. In left plot, the origin of the elliptic coordinate is O, and the elliptic contour represents a surface of $\zeta = \text{const}$, which is mapped to $X = \tilde{X}$ shown in right plot. The vector $\boldsymbol{k}$ points from F_1 to F_2, which correspond to the two foci of the ellipse. Thus an arbitrary vector $\boldsymbol{k}'$ and $\boldsymbol{k} - \boldsymbol{k}'$ can be represented by the vector $\boldsymbol{q}$.

In the elliptic coordinate, the vertex functions defined in Eq. (9) are recasted as

$$\gamma_{112}(\boldsymbol{k} - \boldsymbol{k}', \boldsymbol{k}') = \frac{1 + XY}{(X + Y)^2}, \qquad \gamma_{112}(\boldsymbol{k}' - \boldsymbol{k}, \boldsymbol{k}) = \frac{1 + XY}{4}, \tag{A3}$$

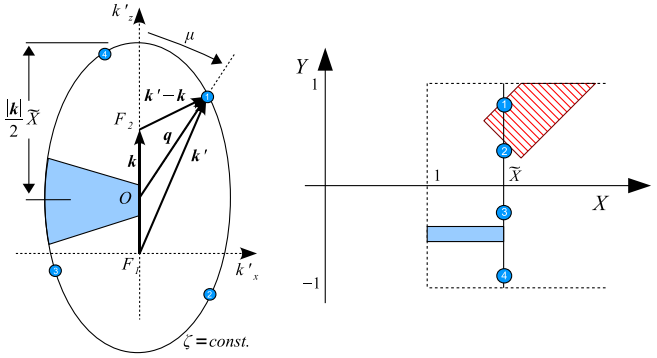

FIG. 7 (color online). The geometrical relation between $\boldsymbol{k}'$ (or $\boldsymbol{q}$) space and (X, Y) coordinates. The elliptic contour representing a surface with $\zeta =$ const. in left plot is mapped to $X = \tilde{X}$ in right plot. Circled numbers in both plots corresponds to each other, and filled areas, too. Note that the origin of $\boldsymbol{k}'$-space is F_1, while that of the elliptic coordinate is O. The striped deficient rectangular is an actual domain defined by Eqs. (A7)–(A10).

$$\gamma_{121}(\boldsymbol{k}-\boldsymbol{k}',\boldsymbol{k}') = \frac{1-XY}{(X-Y)^2}, \qquad \gamma_{121}(\boldsymbol{k}'-\boldsymbol{k},\boldsymbol{k}) = \frac{X^2+Y^2-2}{2(X-Y)^2}, \tag{A4}$$

$$\gamma_{222}(\boldsymbol{k}-\boldsymbol{k}',\boldsymbol{k}') = \frac{2(2-X^2-Y^2)}{(X^2-Y^2)^2}, \qquad \gamma_{222}(\boldsymbol{k}'-\boldsymbol{k},\boldsymbol{k}) = \frac{XY-1}{4}\left(\frac{X+Y}{X-Y}\right)^2. \tag{A5}$$

From now on, we take (X, Y, ϕ) as the integration variables instead of (k'_x, k'_y, k'_z). Hence the volume element $d^3\boldsymbol{k}'$ and the integration domain are changed as

$$\int_{|\boldsymbol{k}'|=k_{\min}}^{|\boldsymbol{k}'|=k_{\max}} \frac{d^3\boldsymbol{k}'}{(2\pi)^3}(\cdots) = \frac{k^3}{32\pi^2}\int_{X_0}^{X_1} dX \int_{Y_0(X)}^{Y_1(X)} dY(\cdots), \tag{A6}$$

Note that, since the integrands of Eqs. (31) and (32) are axially symmetric, we can integrate over the azimuthal angle ϕ, yielding a factor 2π. The lower and upper limits of the integration are determined from the domains of definition of Eqs. (A2) and (25), which gives

$$Y_1(X) = \min\left\{-X + \frac{2k_{m+1}}{k}, X - \frac{2k_{n-1}}{k}, 1\right\}, \tag{A7}$$

$$Y_0(X) = \max\left\{-X + \frac{2k_{m-1}}{k}, X - \frac{2k_{n+1}}{k}, -1\right\}, \tag{A8}$$

$$X_1 = \max\left\{1, \frac{k_{m+1}+k_{n+1}}{k}\right\}, \tag{A9}$$

$$X_0 = \max\left\{1, \frac{k_{m-1}+k_{n-1}}{k}\right\}, \tag{A10}$$

where k_{-1} and k_{N+1} are assigned to $k_0 = k_{\min}$ and $k_N = k_{\max}$, respectively. With the above preparation, the three-dimensional integration (31) and (32) are reduced to two-dimensional integrations over the domain (A7)–(A10). An example of integration domain is depicted as a shaded deficient rectangle in right plot of Fig. 7. As mentioned in Sec. IV, we implement the trapezoidal rule to integrate Eqs. (31) and (32) in this domain.

APPENDIX B: CONVERGENCE TEST

In this appendix, we check the convergence of numerical results obtained with the numerical scheme mentioned in Sec. IV. The test calculations have been done in the ΛCDM model by varying some numerical parameters. Particularly we focus on the initial time of the time evolution, $z_{\rm init}$, and the cutoff wave-number on small scales, $k_{\max}$, introduced in (25), which are most sensitive parameters to the final results.

The upper panel in Fig. 8 shows the fractional errors between the matter power spectrum $P_{11}(k)$ for $k_{\max} = 1, 2, 5h$ Mpc^{-1} and that for $k_{\max} = 10h$ Mpc^{-1} denoted by $P_{11}^{\rm ref}$, that is, $(P_{11} - P_{11}^{\rm ref})/P_{11}^{\rm ref}$. In these calculations, the logarithmic interval $\Delta(\log k)$ is fixed. In the lower panel, we

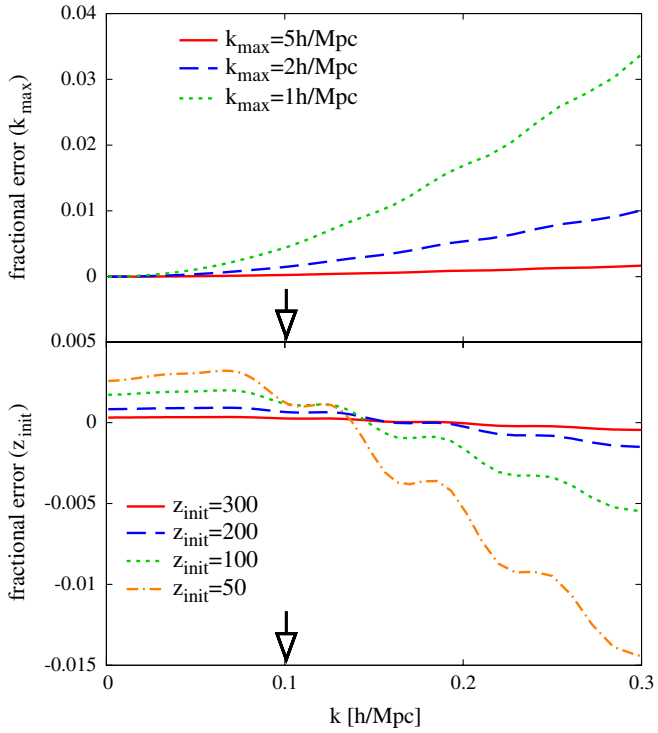

FIG. 8 (color online). The dependence of the cutoff wave number, $k_{\max}$, and the initial time, $z_{\rm init}$, on the matter power spectrum. *Upper panel* : The fractional errors of the power spectrum for $k_{\max} = 5h$ Mpc^{-1} (solid), $k_{\max} = 2h$ Mpc^{-1} (dashed) and $k_{\max} = 1h$ Mpc^{-1} (dotted) by reference to $k_{\max} = 10h$ Mpc^{-1}. *Lower panel* : The fractional errors for $z_{\rm init} = 300$ (solid), $z_{\rm init} = 200$ (dashed), $z_{\rm init} = 100$ (dotted) and $z_{\rm init} = 50$ (dot-dashed) by reference to $z_{\rm init} = 400$. As for the vertical arrows, see the caption of Fig. 4.

show the fractional errors for the calculations with $z_{\rm init} = 50$–300 from the one with $z_{\rm init} = 400$. Also in these calculations, we fixed the time interval, $\Delta\tau$. The arrows on the horizontal axis are given by Eq. (39).

Both plots indicate the good convergence of the numerical results in the sense that the fractional errors from each reference become smaller as $k_{\rm max}$ and $z_{\rm init}$ increase. We found that we can keep the fractional error sufficiently smaller than 1% as long as $k_{\rm max}$ is larger than $5h$ Mpc^{-1}, and $z_{\rm init}$ is larger than 200. Particularly, as for $z_{\rm init}$, if we take later time, the resultant power spectrum at low-redshifts is harmed by the fact that we neglect the decaying modes in the initial conditions [see Eq. (33)].

Considering the above results, we fixed $k_{\rm max} = 5h$ Mpc^{-1} and $z_{\rm init} = 200$ for all numerical calculations presented in this paper. Additionally the number of time steps, N_τ, and the wave number bins, N_k, are chosen as $N_\tau = 172$ and $N_k = 200$, respectively, so that the fractional errors are suppressed to a sub-percent level. Moreover, for the integration (A6), we use a 200×200 discrete grid on the integration domain defined by Eqs. (A7)–(A10).

[1] S. Perlmutter *et al.* (Supernova Cosmology Project), Astrophys. J. **517**, 565 (1999).
[2] D. N. Spergel *et al.* (WMAP), Astrophys. J. Suppl. Ser. **148**, 175 (2003).
[3] G. R. Dvali, G. Gabadadze, and M. Porrati, Phys. Lett. B **485**, 208 (2000).
[4] T. P. Sotiriou and V. Faraoni, arXiv:0805.1726.
[5] M. Tegmark *et al.* (SDSS), Phys. Rev. D **74**, 123507 (2006).
[6] E. Komatsu *et al.* (WMAP), Astrophys. J. Suppl. Ser. **180**, 330 (2009).
[7] M. Crocce and R. Scoccimarro, Phys. Rev. D **73**, 063519 (2006).
[8] M. Crocce and R. Scoccimarro, Phys. Rev. D **73**, 063520 (2006).
[9] P. Valageas, Astron. Astrophys. **465**, 725 (2007).
[10] S. Matarrese and M. Pietroni, J. Cosmol. Astropart. Phys. 06 (2007) 026.
[11] T. Matsubara, Phys. Rev. D **77**, 063530 (2008).
[12] M. Crocce and R. Scoccimarro, Phys. Rev. D **77**, 023533 (2008).
[13] A. Taruya and T. Hiramatsu, Astrophys. J. **674**, 617 (2008).
[14] F. Bernardeau, S. Colombi, E. Gaztañaga, and R. Scoccimarro, Phys. Rep. **367**, 1 (2002).
[15] S. Kida and S. Goto, J. Fluid Mech. **345**, 307 (1997).
[16] T. Nishimichi *et al.*, arXiv:0810.0813.
[17] A. Taruya, T. Nishimichi, S. Saito, and T. Hiramatsu (unpublished).
[18] K. Koyama, A. Taruya, and T. Hiramatsu, arXiv:0902.0618.
[19] J. Khoury and A. Weltman, Phys. Rev. Lett. **93**, 171104 (2004).
[20] P. Valageas, Astron. Astrophys. **421**, 23 (2004).
[21] K. Izumi and J. Soda, Phys. Rev. D **76**, 083517 (2007).
[22] M. Pietroni, J. Cosmol. Astropart. Phys. 10 (2008) 036.
[23] F. Bernardeau, M. Crocce, and R. Scoccimarro, Phys. Rev. D **78**, 103521 (2008).
[24] D. Jeong and E. Komatsu, Astrophys. J. **651**, 619 (2006).
[25] T. Nishimichi *et al.*, arXiv:0705.1589.
[26] D. Jeong and E. Komatsu, Astrophys. J. **691**, 569 (2009).
[27] M. Chevallier and D. Polarski, Int. J. Mod. Phys. D **10**, 213 (2001).
[28] E. V. Linder, Phys. Rev. Lett. **90**, 091301 (2003).
[29] S. Hannestad and E. Mortsell, J. Cosmol. Astropart. Phys. 09 (2004) 001.
[30] R. Takahashi, Prog. Theor. Phys. **120**, 549 (2008).
[31] E. Sefusatti and E. Komatsu, Phys. Rev. D **76**, 083004 (2007).
[32] C. Sealfon, L. Verde, and R. Jimenez, Phys. Rev. D **71**, 083004 (2005).
[33] A. Shirata, T. Shiromizu, N. Yoshida, and Y. Suto, Phys. Rev. D **71**, 064030 (2005).
[34] A. Shirata, Y. Suto, C. Hikage, T. Shiromizu, and N. Yoshida, Phys. Rev. D **76**, 044026 (2007).
[35] W. Hu and I. Sawicki, Phys. Rev. D **76**, 064004 (2007).
[36] A. A. Starobinsky, JETP Lett. **86**, 157 (2007).
[37] S. A. Appleby and R. A. Battye, Phys. Lett. B **654**, 7 (2007).
[38] H. Oyaizu, M. Lima, and W. Hu, Phys. Rev. D **78**, 123524 (2008).
[39] H. Oyaizu, Phys. Rev. D **78**, 123523 (2008).
[40] F. Schmidt, M. V. Lima, H. Oyaizu, and W. Hu, Phys. Rev. D **79**, 083518 (2009).
[41] J. Lesgourgues, S. Matarrese, M. Pietroni, and A. Riotto, arXiv:0901.4550.